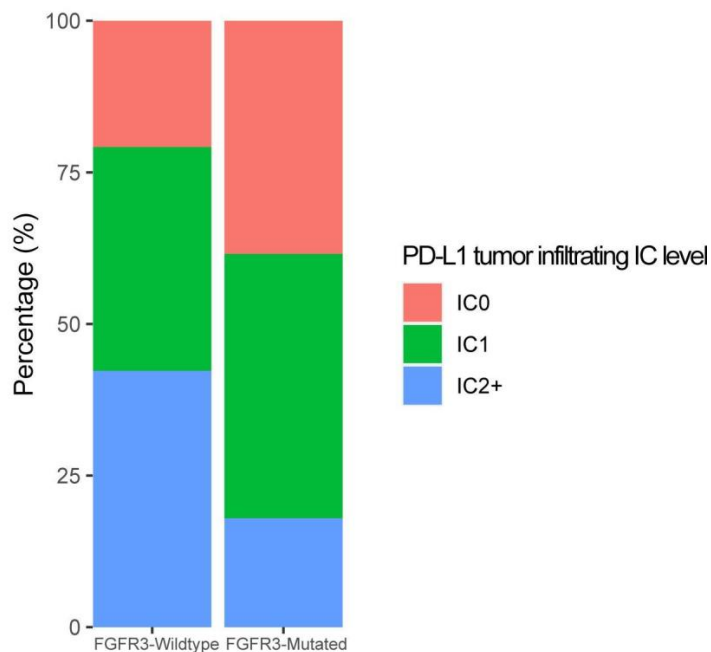
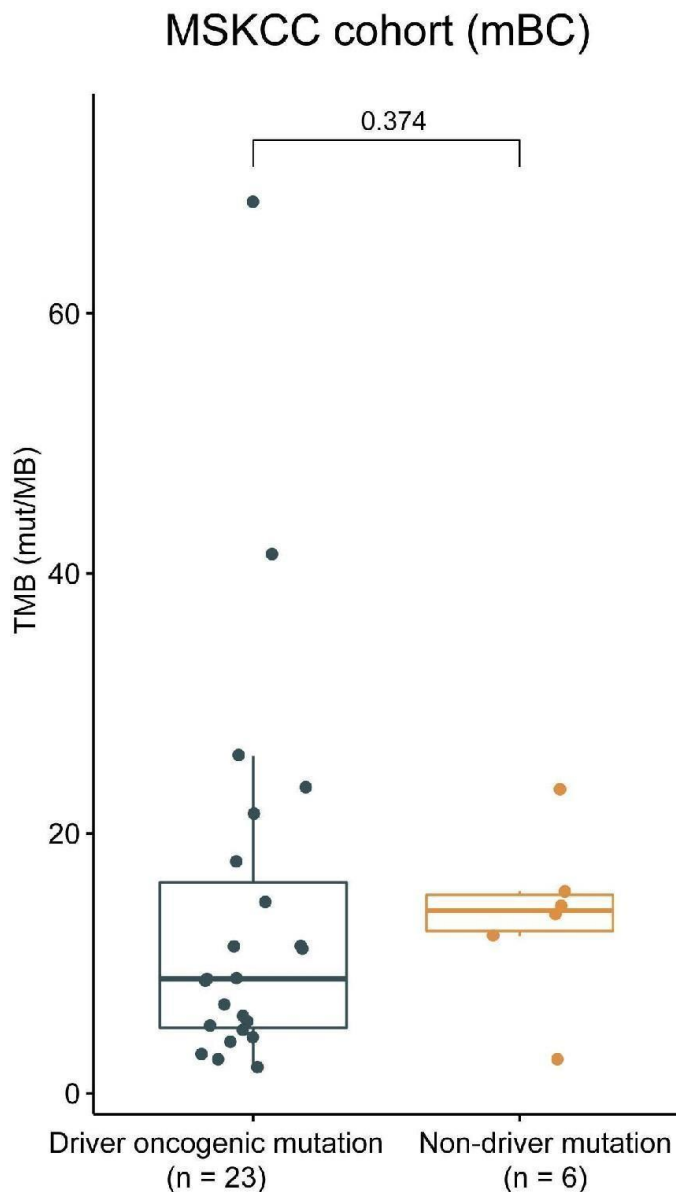


## Supplementary Figures



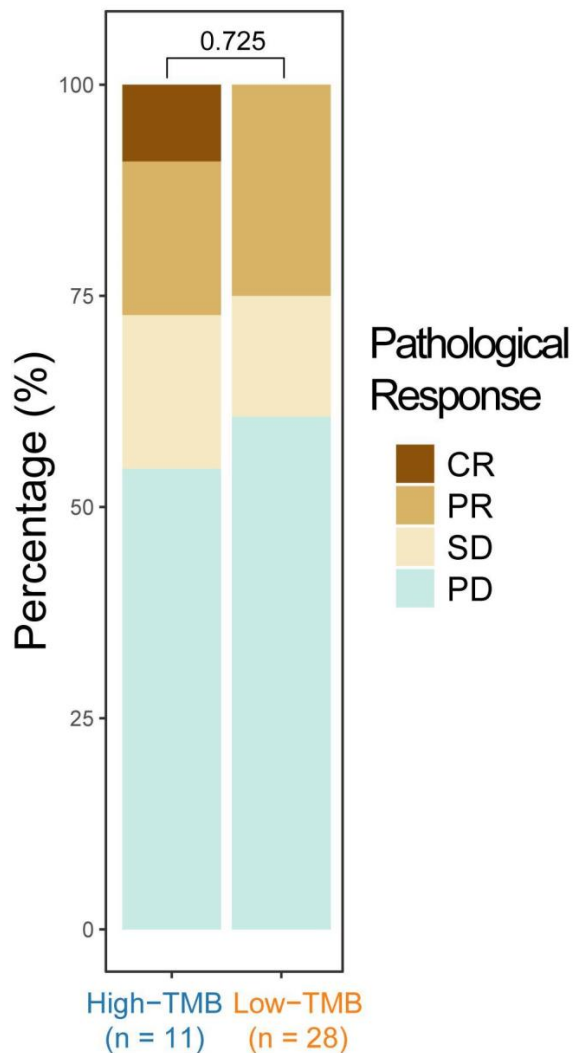
**Supplementary Figure 1.** FGFR3 mutation group carried a lower proportion of IC1 and IC2+ than FGFR3 wildtype group (61.5% versus 79.2%,  $P=0.021$ ) in IMvigor210 cohort. Data were analyzed by chi-square test. PD-L1, programmed death ligand 1; IC, immune cell.



**Supplementary Figure 2.** Patients with driver oncogenic mutations in FGFR3 (median TMB=8.8, IQR=5.0-16.2) carried a trend toward lower TMB in comparison to those with non-driver FGFR3 mutations (median TMB=14.1, IQR=12.5-15.3) in MSKCC (mBC) immunotherapy cohort, although not statistically significant (P=0.374). Data were analyzed by Wilcoxon test.

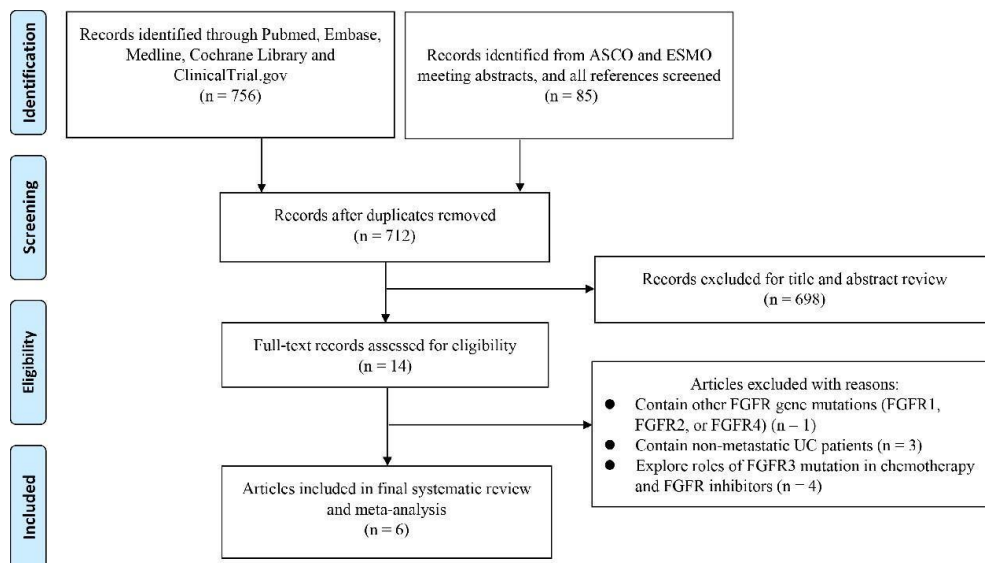
IQR, interquartile range; TMB, tumor mutation burden; MSKCC, Memorial Sloan Kettering Cancer Center; mBC, metastatic bladder cancer

Patients with driver oncogenic mutations in FGFR3 (n=39)  
IMVigor210 cohort



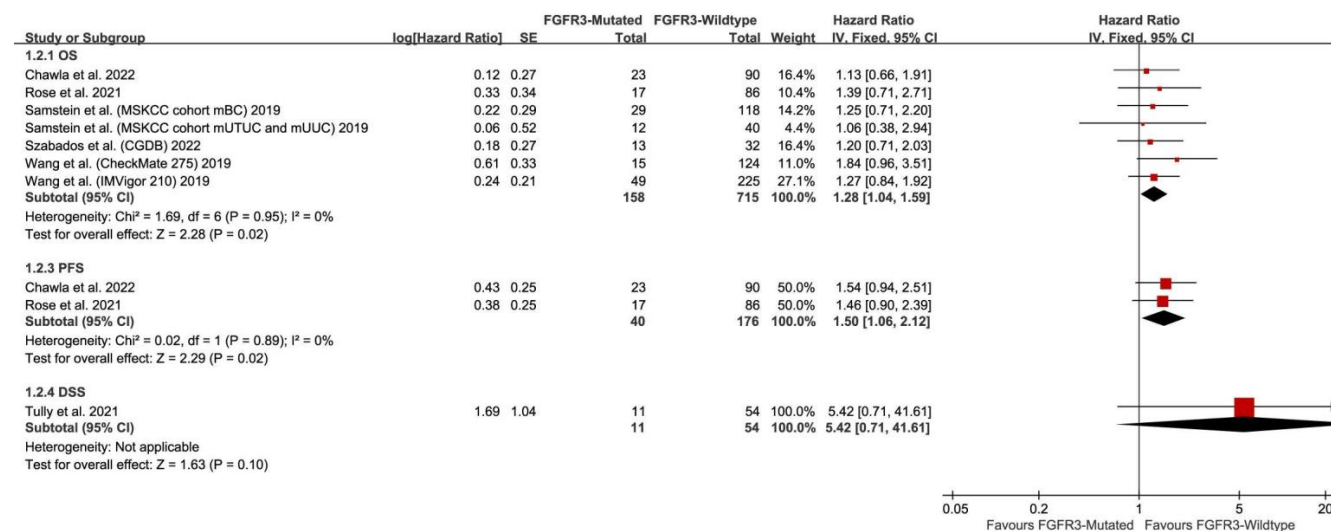
**Supplementary Figure 3.** Disease control rates were similar between high-TMB ( $\geq 10$  mut/MB) and low-TMB ( $<10$  mut/MB) groups in patients with driver FGFR3 oncogenic mutations based on IMvigor210 immunotherapy cohort (45.5% versus 39.3%,  $P=0.725$ ). Data were analyzed by chi-square test.

CR, complete response; PR, partial response; SD, stable disease; PD, progressive disease; TMB, tumor mutation burden.



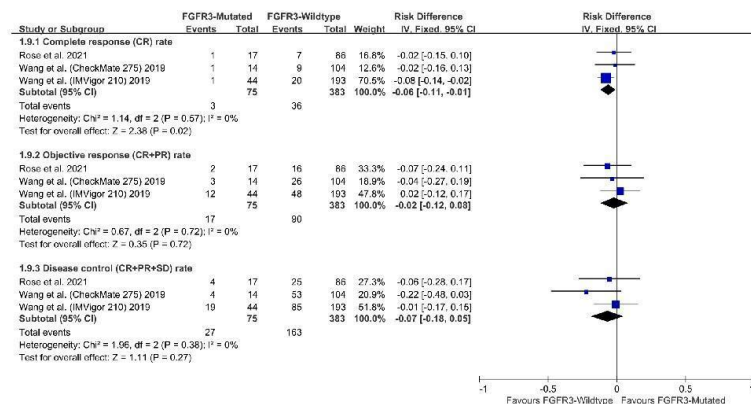
**Supplementary Figure 4.** The Preferred Reporting Items for Systematic Reviews and Meta-analyses flow diagram.

ESMO, European Society of Medical Oncology; ASCO, American Society of Clinical Oncology; UC, urothelial carcinoma.

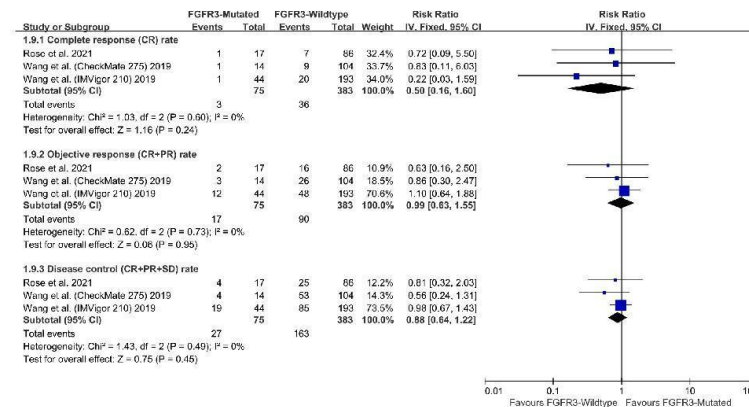


**Supplementary Figure 5.** Forest plots showing FGFR3-mutated metastatic urothelial carcinoma patients had similar progression free survival (PFS) and disease specific survival (DSS) to FGFR3-wildtype patients after immune checkpoint blockade treatment. CI, confidence interval.

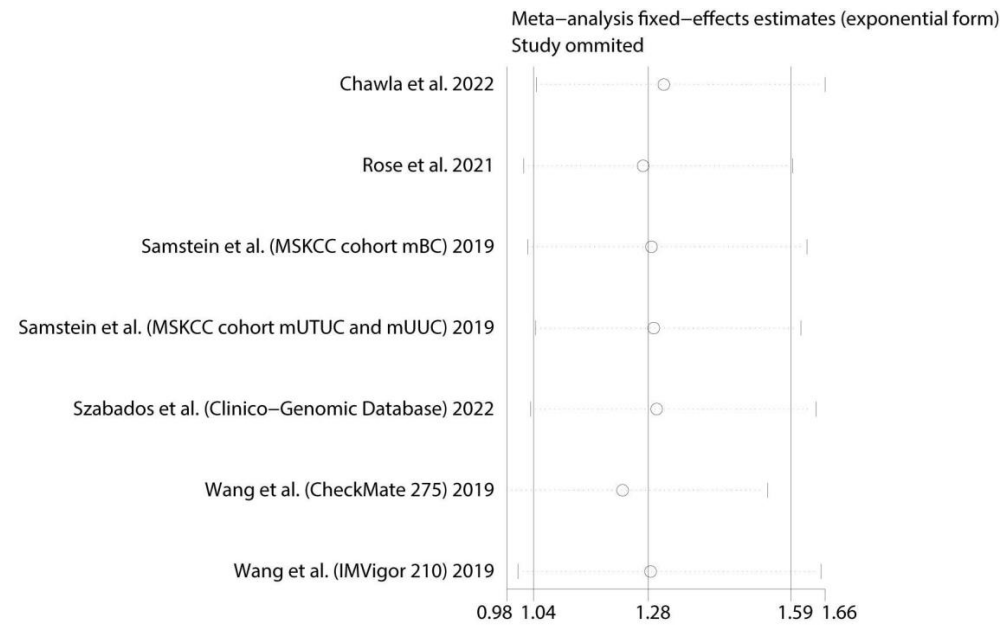
A



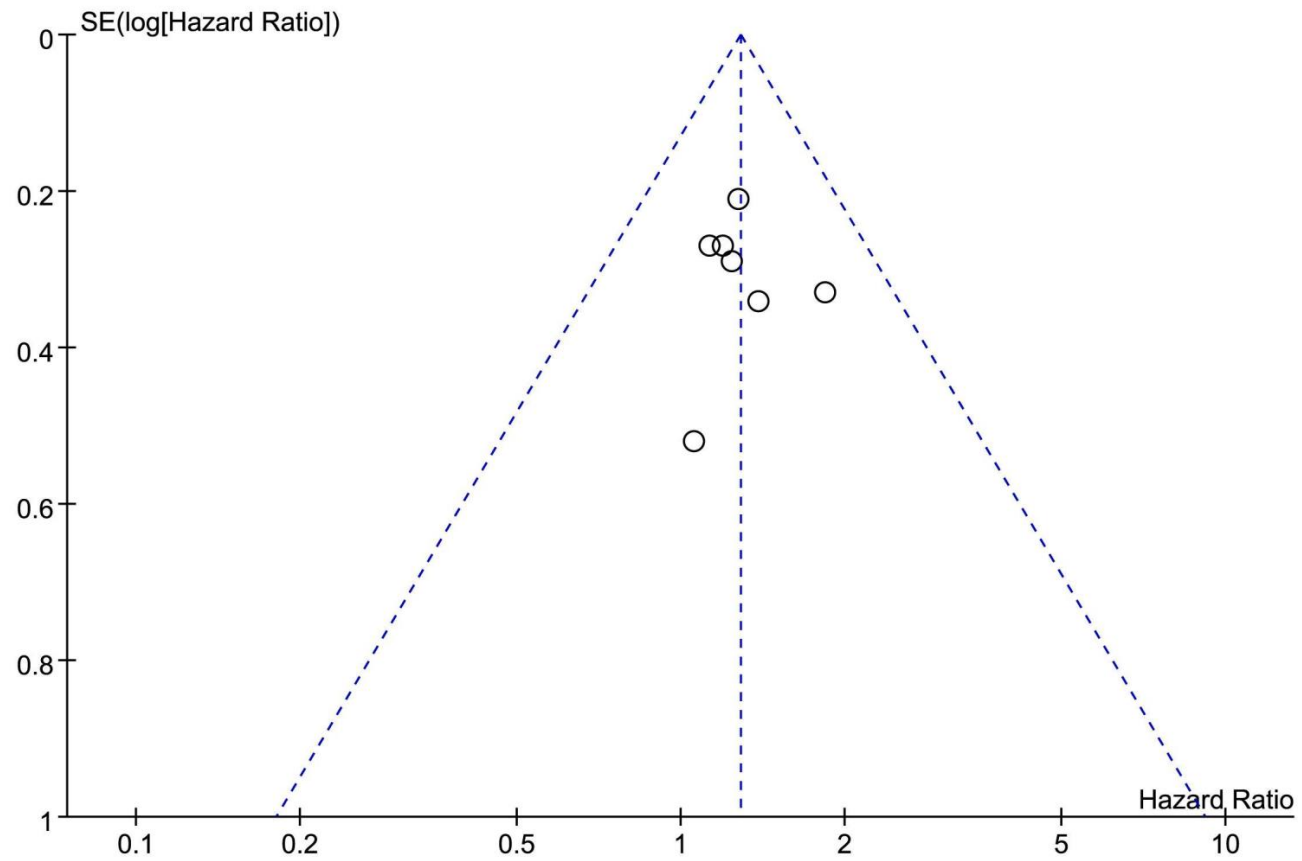
B



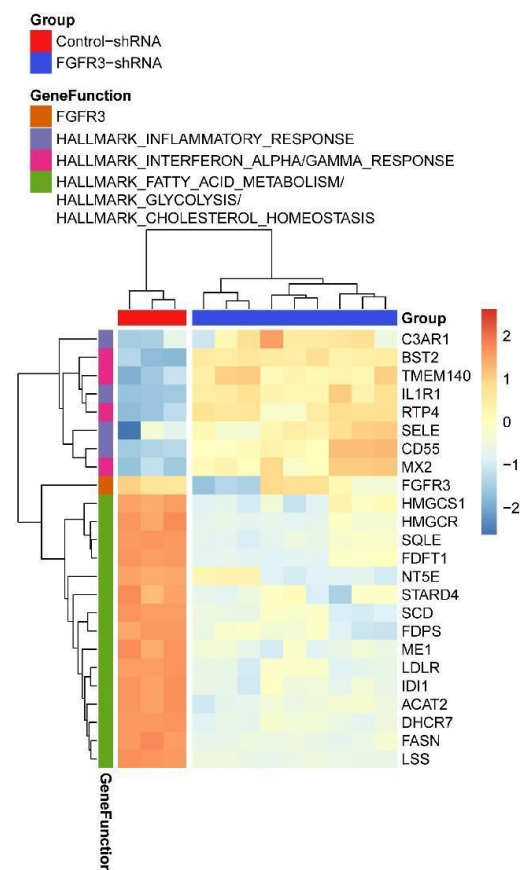
**Supplementary Figure 6.** Forest plots showing FGFR3-mutated metastatic urothelial carcinoma patients had lower complete response rate than FGFR3-wildtype patients after immune checkpoint blockade treatment. (A) Forest plots evaluated by risk difference. (B) Forest plots evaluated by risk ratio. CR, complete response; PR, partial response; SD, stable disease; CI, confidence interval.



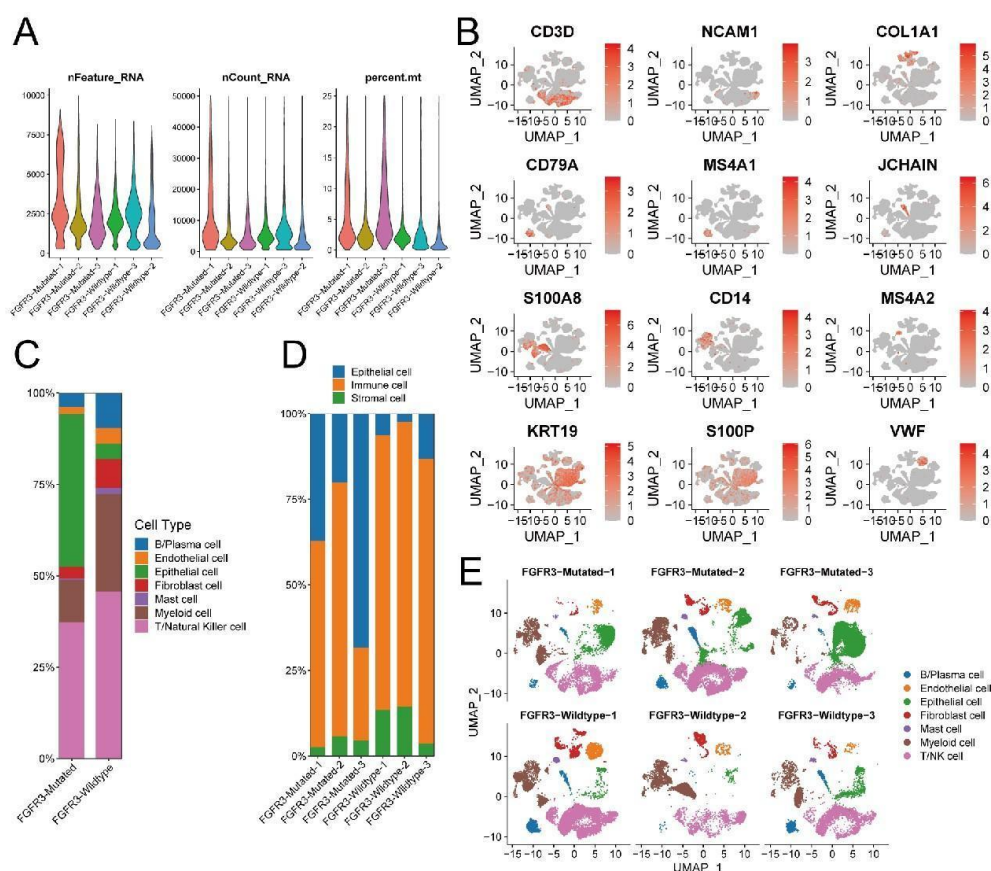
**Supplementary Figure 7.** Sensitivity analysis including all six studies of FGFR3 mutation on overall survival in metastatic urothelial carcinoma patients after immune checkpoint blockade treatment.



**Supplementary Figure 8.** Funnel plot for publication bias. Funnel plot including all six studies of FGFR3 mutation on overall survival in metastatic urothelial carcinoma patients after immune checkpoint blockade treatment.

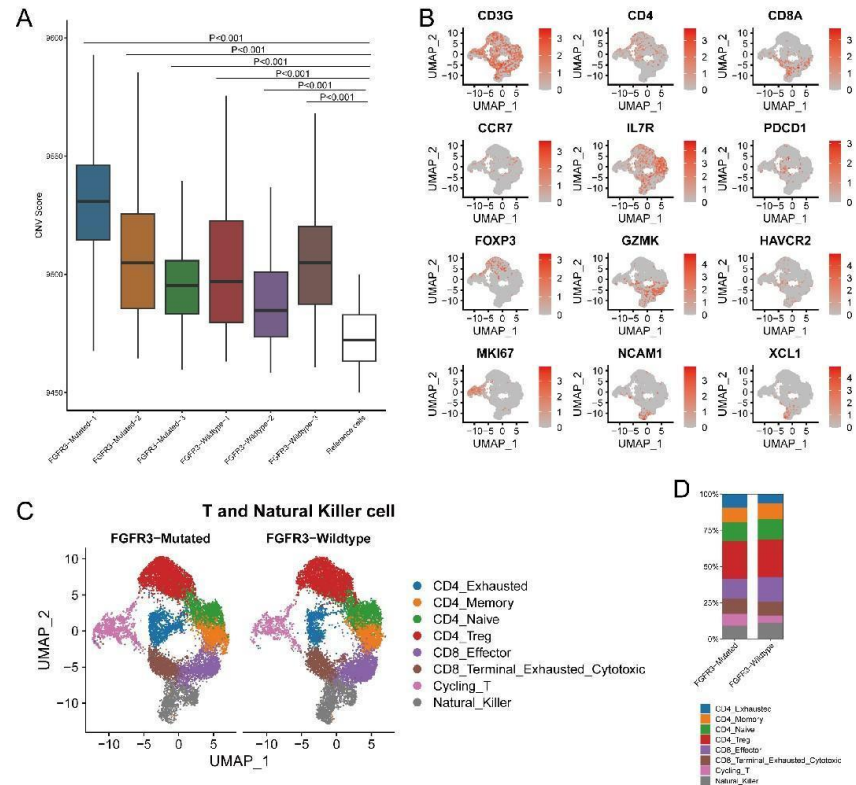


**Supplementary Figure 9.** Heatmap for immune-related and metabolism-related differential expressed genes between control-shRNA and FGFR3-shRNA RT-112 bladder cancer cell lines. shRNA, short hairpin RNA.



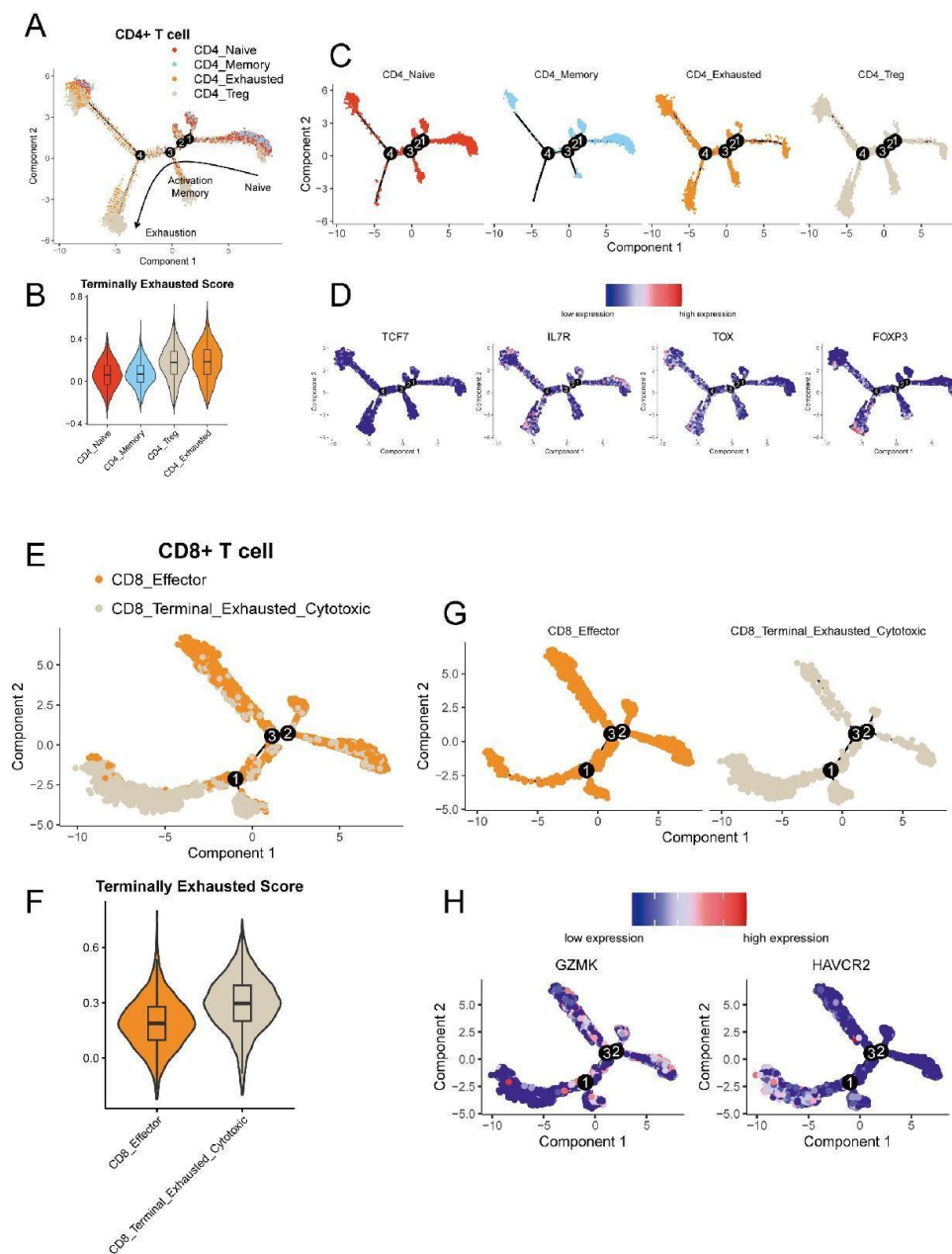
**Supplementary Figure 10.** Single-cell RNA sequencing decoded FGFR3-mutated UC and FGFR3-wildtype UC.

(A) Violin plots showed number of genes (nFeature\_RNA) detected, number of UMI (nCount\_RNA), and percent of mitochondrial derived transcripts (percent.mt) per single cell for quality control. (B) UMAP plots, color-coded for the expression (gray to red) of marker genes for each cell type, as indicated. (C) Histogram showed the relative proportions of cells in FGFR3-mutated and FGFR3-wildtype tumors. (D) Histogram showed the relative proportions of cells in every tumor sample. (E) UMAP plots showed cell origins by each tumor sample.



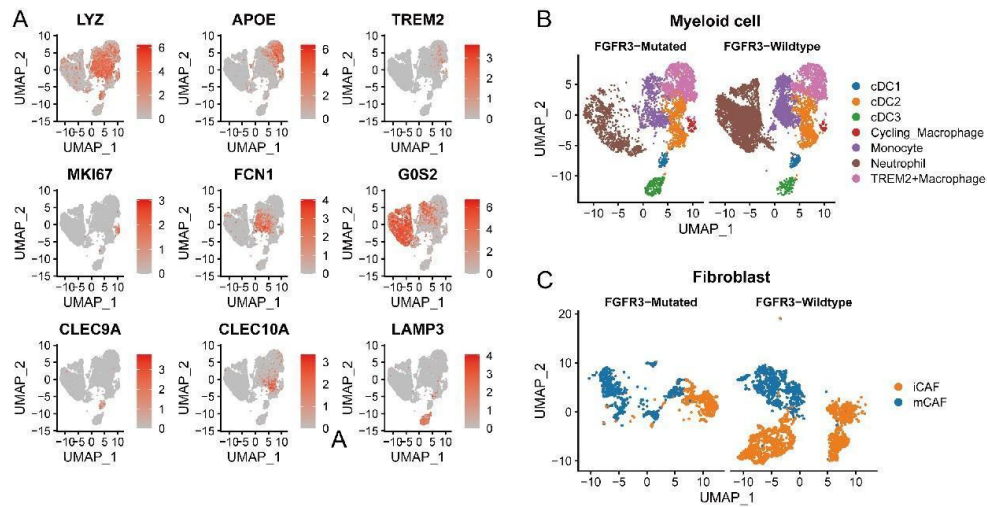
**Supplementary Figure 11.** Single-cell RNA sequencing decoded the Epithelial and T cells between FGFR3-mutated UC and FGFR3-wildtype UC.

(A) Calculated CNV scores of epithelial cells and reference cells. Epithelial cells in each patient carry higher CNV scores than reference cells, which indicated all epithelial cells are all malignant cells. (B) UMAP plots, color-coded for the expression (gray to red) of marker genes for each T cell subtype, as indicated. (C) UMAP plots showed T cell origins by FGFR3 mutation status. (D) Histogram showed the relative proportions of T cell subtypes in each tumor sample.



**Supplementary Figure 12.** Developmental trajectory analysis of CD4+ T cells and CD8+ T cells.

(A) Developmental trajectory of CD4+ T cells. (B) Violin plots showed the terminally exhausted score between CD4+ T cell subtypes. (C) Each CD4+ T cell subtype in developmental trajectory. (D) TCF7 (naive marker), IL7R (memory marker), TOX (exhausted marker), and FOXP3 (Treg marker) expression in CD4+ T cell developmental trajectory. (E) Developmental trajectory of CD8+ T cells. (F) Violin plots showed the terminally exhausted score between CD8+ T cell subtypes. (G) Each CD8+ T cell subtype in developmental trajectory. (H) GZMK (effector marker) and HAVCR2 (terminally exhausted marker) in CD8+ T cell developmental trajectory.



**Supplementary Figure 13.** Single-cell RNA sequencing decoded the myeloid and fibroblast cells between FGFR3-mutated UC and FGFR3-wildtype UC. (A) UMAP plots, color-coded for the expression (gray to red) of marker genes for each myeloid cell subtype, as indicated. (B) UMAP plots showed myeloid cell origins by FGFR3 mutation status. (C) UMAP plots showed fibroblast cell origins by FGFR3 mutation status.

